IMPROVING THE CLASSIFICATION IN SHADOWED AREAS USING NONLINEAR SPECTRAL UNMIXING

Guichen Zhang, Daniele Cerra, Rupert Müller

German Aerospace Center (DLR)
Remote Sensing Technology Institute (IMF)
82234 Wessling, Germany

ABSTRACT

This paper presents a shadow restoration method based on the nonlinear mixture model. A shadowed spectrum is modeled by using a pure sunlit spectrum for the same material following physical assumptions. Regarding pure sunlit and shadowed spectra as endmembers, an unmixing process is then conducted pixel-wise using a nonlinear mixture model. Shadow pixels are restored by simulating their exposure to sunlight through a combination of selected sunlit endmembers spectra, weighted by abundance values. Experiments conducted on a real airborne hyperspectral image are evaluated through spectra comparison and classification. In addition, a soft shadow map is generated, which quantifies the shadow intensity at the edges between sunlit and shadow areas.

Index Terms— shadow restoration, hyperspectral, spectral unmixing

1. INTRODUCTION

Hyperspectral images contain rich spectral information and have been widely used in remote sensing applications [1]. In airborne hyperspectral images in the visible (VIS) and near-infrared (NIR) ranges, cast shadow is frequently visible [2]. As shadow pixels lack direct sun illumination compared to sunlit pixels, their computed reflectance values can be incorrect, if these are not processed separately in the atmospheric correction step. Therefore, it is of great interest to compute correct reflectance values in shadow areas.

Previous works have studied shadow mask generation or shadow removal from remote sensing images. Mostly, shadow masks were generated and used as input for shadow removal [2]. Three categories of shadow detection methods can be distinguished, which are thresholding, studying of the geometry and light source of the scene, and computing indices which are insensitive to shadow [2]. Besides shadow detection, shadow restoration has also been an active research field. Some works consider the relation of statistics or brightness distribution between paired shadow and sunlit regions for the shadow removal of true color images [3, 4]. Recently,

deep learning based shadow detection and removal methods have been proposed [5], which require large training sets of shadow and shadow-free images.

Furthermore, other methods for recovering shadow in hyperspectral images have been investigated. Roussel et al. assume that the spectral angle of sunlit and shadow pixels with the same material is small, which reduces deshadowing to a pixel matching problem [6, 7]. Physical based methods relying on a nonlinear unmixing method modeled shadow effect through multiple scattering of incident light [8]. Besides, field experiments have found out that the spectral ratio between shadow and sunlit pixels for the same material decreases as the acquisition wavelength increases [9].

Other approaches based on spectral unmixing aim at decomposing an image pixel into pure material spectra, i.e. endmembers, and their corresponding spatial proportion, i.e. abundances. So far, several spectral unmixing methods regard shadows as an endmember, whose spectral values at all wavelengths are zeros [1]. Recently, we proposed a shadow restoration method based on nonlinear unmixing model and physical assumptions [10]. By considering the differences of irradiance in sunlit and shadow pixels, this method models the spectrum in the shadow using the spectrum of the same material under sunlight. We defined pure spectra under sunlight and their modeled spectra in the shadow as sunlit and shadowed endmembers, repectively. Subsequently, abundances values through a nonlinear unmixing process were derived. Finally, shadow restoration could be conducted through pixel reconstruction.

In this paper, we present an improvement on [10]. The main novelty is a power function used to model the ratio between diffused irradiance and direct sun irradiance on the ground. Furthermore, a post-processing step is introduced to mitigate over-fitting. Restoration result are assessed quantitatively by comparing spectral distances and classification results.

2. METHOD

In our previous work [10], we assumed sunlit pixels in an image to receive both direct and diffuse sun irradiance, while shadowed pixels are illuminated only the latter. Thus, we modeled the pure spectrum of a material in the shadow, i.e. a shadow endmember, using a the pure spectrum of the same material under sunlight, i.e. a sunlit endmember, allowing for some variability in the endmember. A detailed description can be found in [10]. Instead of modeling nonlinear effect through a second-order polynomial model [11] with a free parameter b as in our previous work, a Fan model [12] is applied in this paper in order to reduce over-fitting. The reflectance r_s of a material in shadow is then reconstructed as:

$$r_s(\lambda) = \frac{E_s(\lambda)}{E_l(\lambda)} \cdot r_l + \frac{E_s(\lambda)}{E_l(\lambda)} \cdot \sum_{i=1}^{p-1}\sum_{j=i+1}^{p} a_i \cdot a_j \cdot r_{l,i}(\lambda) \cdot r_{l,j}(\lambda),$$

(1)

where $E_l(\lambda)$ represents the direct irradiance at wavelength λ, $E_s(\lambda)$ the diffused irradiance at wavelength λ, p is the number of materials (endmembers) in one pixel, $r_{l,i}(\lambda)$ the i-th reflectance of a sunlit material (endmember) at wavelength λ, and a_i is the i-th abundance corresponding to $r_{l,i}$.

Here, $\frac{E_s(\lambda)}{E_l(\lambda)}$ is the ratio between diffuse sun irradiance and direct sun irradiance on the ground. In this paper, we model this ratio as a power function $k_1\lambda^{-k_2} + k_3$ instead of λ^{-4}, as the function related to Rayleigh scattering may not hold alone for real cases, even in the clearest sky. This is due to, among other factors, humidity and dust content [13]. With the assumption that atmosphere conditions do not change across a single airborne image, all parameters k_1,k_2, and k_3 are constant. Another free parameter F, representing how much diffused irradiance a pixel receives, is estimated pixel by pixel. The described ratio is then computed as:

$$\frac{E_s(\lambda)}{E_l(\lambda)} = F \cdot (k_1\lambda^{-k_2} + k_3)$$

(2)

where λ is a wavelength, k_1, k_2, k_3 are positive parameters, and F ranges from 0 to 1.

We represent equation (1) and (2) in vector form, in order to solve for all wavelengths simultaneously. Note that $\boldsymbol{e\_l_i}$ is the i-th sunlit endmember, where $i = 1, 2, ...p$, with p the total number of endmembers, a_l_i the i-th abundance corresponding to the i-th sunlit endmember, and a_s_i the i-th abundance corresponding to the i-th shadowed endmember. Given an i-th sunlit endmember $\boldsymbol{e\_l_i}$, a corresponding shadowed endmember $\boldsymbol{e\_s_i}$ can be written as:

$$\boldsymbol{e\_s_i} = F \cdot (k_1\boldsymbol{\lambda}^{-k_2} + k_3) \cdot \boldsymbol{e\_l_i} +$$
$$F \cdot (k_1\boldsymbol{\lambda}^{-k_2} + k_3) \cdot \sum_{i=1}^{p-1}\sum_{j=i}^{p} a_i \cdot a_j \cdot \boldsymbol{e\_l_i} \cdot \boldsymbol{e\_l_j}$$

(3)

Nonlinear effects of sunlit endmembers $\boldsymbol{e\_l_i}$ are considered through the FAN model [12]. For a pixel $\boldsymbol{x}$ we have:

$$\boldsymbol{x} = \sum_{i=1}^{p} a\_l_i \cdot \boldsymbol{e\_l_i} + \sum_{i=1}^{p} a\_s_i \cdot \boldsymbol{e\_s_i}$$
$$+ \sum_{i=1}^{p-1}\sum_{j=i+1}^{p} a\_l_i \cdot a\_l_j \cdot \boldsymbol{e\_l_i} \cdot \boldsymbol{e\_l_j}$$

(4)

where $\sum_{i=1}^{p} a\_l_i + a\_s_i = 1$, $a\_l_i \geq 0$, and $a\_s_i \geq 0$.

As a_s_i and a_l_i are the abundances of shadowed and sunlit endmembers for the same material, the shadow restoration result $\boldsymbol{x_{restore}}$ of pixel $\boldsymbol{x}$ with B spectral bands is computed by:

$$\boldsymbol{x_{restore}} = \sum_{i=1}^{p} (a\_l_i + a\_s_i) \cdot \boldsymbol{e_i}$$
$$+ \sum_{i=1}^{p-1}\sum_{j=i+1}^{p} a\_l_i \cdot a\_l_j \cdot \boldsymbol{e\_l_i} \cdot \boldsymbol{e\_l_j}$$

(5)

3. EXPERIMENTAL RESULTS

We analyze an image subset from an airborne hyperspectral image acquired over Oberpfaffenhofen, Bavaria, Germany (Fig. 4 (a)) with a HySpex VNIR sensor flying at an altitude of 1615 m, resulting in an image of 181×245 pixels, with a ground sampling distance of 0.7 m. The image comprises 160 spectral bands ranging from 416 nm to 988.4 nm and has been atmospherically corrected using ATCOR [14]. After removing water vapor bands, a total of 101 bands have been processed (Fig. 4 (b)). Six pairs of sunlit and shadowed pure pixels distributed over the whole image have been manually selected. The parameters $k_1 = 1.29$, $k_2 = -7.14$, and $k_3 = 0.49$ in equation (2) have been computed through least-squares estimation.
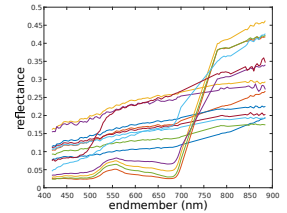
(a) image in true color composite   (b) endmembers

Fig. 1. Hyperspectral image and manually-selected endmembers from sunlit pixels.

Abundances and F maps were then estimated using the proposed model in equation (4). For sunlit pixels, only the terms containing sunlit abundances in equation (4) should be larger than 0, but in practice shadowed abundances and F values are also used to minimize the objective function, resulting in an over-fitting of equation (4) in sunlit pixels. Therefore, a

2409

sunlit mask is generated in order to separate pure sunlit from shadowed and sun-shade pixels based on residual analysis, where we define a sun-shade pixel as a mixed pixel of sunlit and shadowed pixels.

Firstly, we decompose equation (4) into two sub-equations by separating the terms of sunlit and shadowed abundances, resulting in $x = \sum_{i=1}^{p} a\_s_i \cdot e\_s_i$ noted as a shadowed equation, and $x = \sum_{i=1}^{p} a\_l_i \cdot e\_l_i + \sum_{i=1}^{p-1} \sum_{j=i+1}^{p} a\_l_i \cdot a\_l_j \cdot e\_l_i \cdot e\_l_j$ noted as a sunlit equation. We have observed that the reconstruction computed from the sunlit or shadowed equation is close to the one computed from equation (4) in the spectral domain, if the input pixel x is a pure sunlit or shadowed pixel, respectively. Instead, the reconstruction uses both sunlit and shadowed terms if the input pixel x is a sun-shade pixel, or if x is a new material. We separate sun-shade pixels and new materials through a morphological opening, with the assumption that sun-shade borders appear as thin lines in a local neighborhood, while new materials span larger and more compact areas. Consequently, a ratio indicating the spectral distances of the above reconstruction results resulted in a sunlit factor map (Fig.2 (d)). A hard threshold of 0.9 was set, with F values set to zero in the mask (Fig. 2 (c)).

A total of 19 endmembers have been chosen, with some of them being spectrally similar to account for spectral variability. The five sunlit and shadowed materials abundance maps aggregate several endmembers belonging to similar materials (Fig. 3), and show that sunlit and shadowed abundances have been generated successfully. With the advantage of spectral unmixing, analyzing materials at sub-pixel level, a sunlit fraction map considering border pixels between sunlit and shadow areas has been also computed by summing up the abundances of sunlit endmembers. Instead of a binary mask, Fig. 2 (a)-(b) show a soft border between sun and shadow areas, yielding a more realistic representation of shadows.

In Fig. 4 (a) reflectance in most shadow areas appears to have been recovered. We validated results quantitatively by analyzing ten pairs of sun-shadow image elements from the scene. In each pair, we have assumed that sunlit and shadow areas that are close to the sun-shade border belong to a same material. Fig. 4 (e) shows that spectral distances for each pair of sunlit and shadow areas significantly decrease after applying the proposed method. We additionally validate our method by comparing classification results in Fig. 4. We applied a Support Vector Machine (SVM) classifier with default settings (radial basis function with $gamma = 0.01$) as available in ENVI software (version 5.5). We selected 1417 training samples (17% grass, 63% trees, and 20% impervious surfaces) and 1489 validation samples (17% grass, 47% trees, and 35% impervious surfaces). After shadow restoration, the overall accuracy and k score increased from 73% to 99% and from 0.55 to 0.99, respectively. The producer accuracy of grass and impervious surfaces increased from 44% to 100% and from 53% to 98%, respectively.
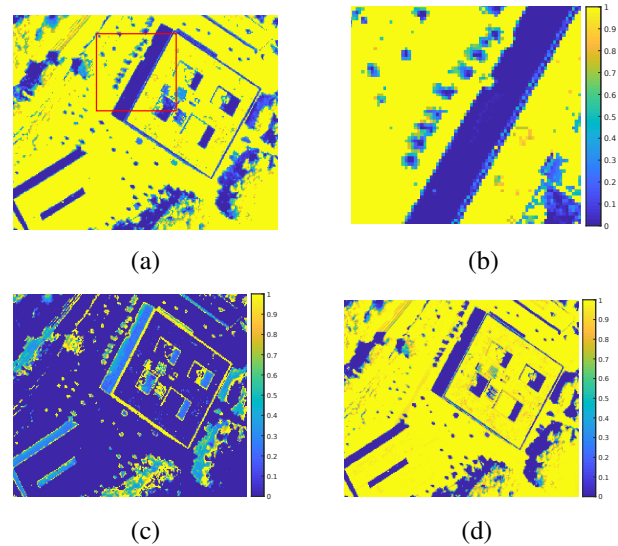

Fig. 2. Computed parameters. (a) total abundances of sunlit endmembers; (b) detail of image (a); (c) F parameter; (d) sunlit factor.
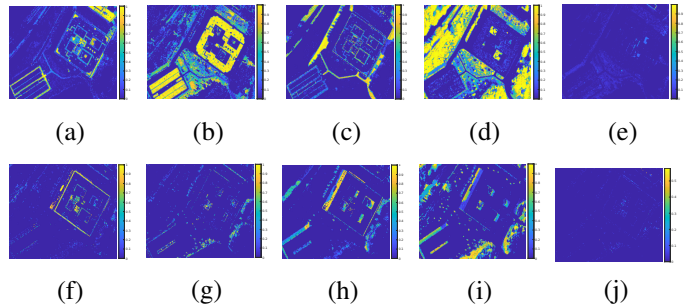

Fig. 3. Abundance maps of sunlit endmembers: (a) roof1, (b) roof2, (c) road, (d) vegetation, (e) man-made material. Abundance maps of shadowed endmembers: (f) roof1, (g) roof2 (h) road, (i) vegetation, (j): man-made material.

4. CONCLUSION

This paper presents an improved shadow restoration method using nonlinear spectral unmixing and physical assumptions based on our previous work [10]. The method was tested on a real hyperspectral airborne image. Results show that the proposed method successfully recovers spectral information in shadow areas. When comparing the restored image with the input image, the spectral distance between sunlit and shadowed pixels for a given material decrease largely. Moreover, classification accuracy for a simple case improves from 73% to 99% after our spectral restoration.
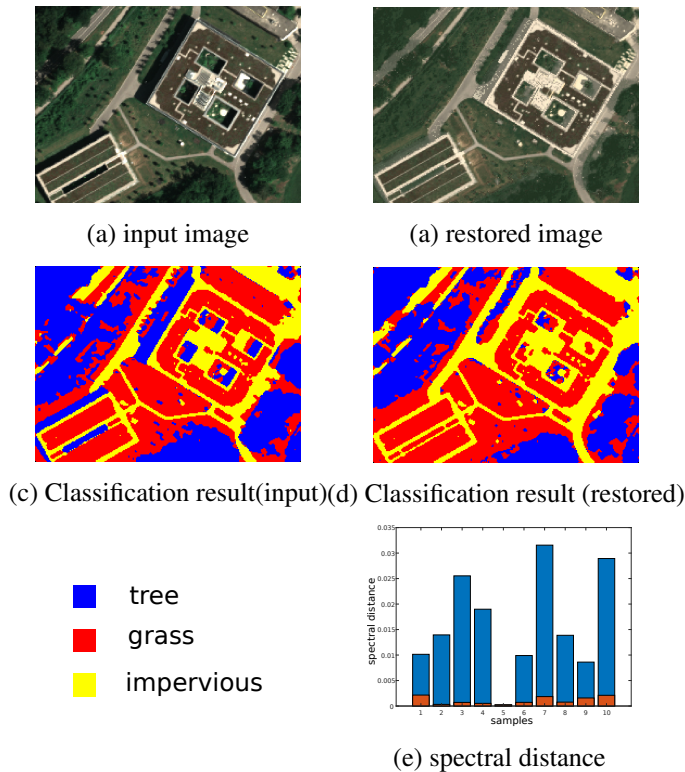
(a) input image

(a) restored image

(c) Classification result(input)(d) Classification result (restored)

tree

grass

impervious

(e) spectral distance

Fig. 4. (a) Input image in true color composite; (b) Restored image in true color composite; (c) classification result of input image; (d) classification result of restored image; (e) spectral euclidean distance between sunlit and shadow pixels: from input image in blue color; from restored image in red color

5. REFERENCES

[1] Nicolas Dobigeon, Jean-Yves Tourneret, Cédric Richard, José Carlos M Bermudez, Stephen McLaughlin, and Alfred O Hero, "Nonlinear unmixing of hyperspectral images: Models and algorithms," *IEEE Signal Processing Magazine*, vol. 31, no. 1, pp. 82–94, 2013.

[2] AmirReza Shahtahmassebi, Ning Yang, Ke Wang, Nathan Moore, and Zhangquan Shen, "Review of shadow detection and de-shadowing methods in remote sensing," *Chinese Geographical Science*, vol. 23, no. 4, pp. 403–420, 2013.

[3] Takashi Nakajima, Guo Tao, and Yoshifumi Yasuoka, "Simulated recovery of information in shadow areas on ikonos image by combing als data," 2002.

[4] P. Sarabandi, F. Yamazaki, M. Matsuoka, and A. Kiremidjian, "Shadow detection and radiometric restoration in satellite high resolution images," in *IGARSS 2004. 2004 IEEE International Geoscience and Remote Sensing Symposium*, Sep. 2004, vol. 6, pp. 3744–3747 vol.6.

[5] Liangqiong Qu, Jiandong Tian, Shengfeng He, Yandong Tang, and Rynson WH Lau, "Deshadownet: A multi-context embedding deep network for shadow removal," in *Proceedings of the IEEE Conference on Computer Vision and Pattern Recognition*, 2017, pp. 4067–4075.

[6] Guillaume Roussel, Christiane Weber, Xavier Ceamanos, and Xavier Briottet, "A sun/shadow approach for the classification of hyperspectral data," in *2016 8th Workshop on Hyperspectral Image and Signal Processing: Evolution in Remote Sensing (WHISPERS)*. IEEE, 2016, pp. 1–5.

[7] Moussa Sofiane Karoui and Khelifa Djerriri, "A new unmixing-based approach for shadow correction of hyperspectral remote sensing data," in *IGARSS 2018-2018 IEEE International Geoscience and Remote Sensing Symposium*. IEEE, 2018, pp. 2725–2728.

[8] Rob Heylen, Vera Andrejchenko, Zohreh Zahiri, Mario Parente, and Paul Scheunders, "Nonlinear hyperspectral unmixing with graphical models," *IEEE Transactions on Geoscience and Remote Sensing*, 2019.

[9] F. Yamazaki, W. Liu, and M. Takasaki, "Characteristics of shadow and removal of its effects for remote sensing imagery," in *2009 IEEE International Geoscience and Remote Sensing Symposium*, July 2009, vol. 4, pp. IV–426–IV–429.

[10] G. Zhang, D. Cerra, and R. Muller, "Towards the spectral restoration of shadowed areas in hyperspectral images based on nonlinear unmixing," in *2019 10th Workshop on Hyperspectral Imaging and Signal Processing: Evolution in Remote Sensing (WHISPERS)*, Sep. 2019, pp. 1–5.

[11] Yoann Altmann, Abderrahim Halimi, Nicolas Dobigeon, and Jean-Yves Tourneret, "Supervised nonlinear spectral unmixing using a postnonlinear mixing model for hyperspectral imagery," *IEEE Transactions on Image Processing*, vol. 21, no. 6, pp. 3017–3025, 2012.

[12] Wenyi Fan, Baoxin Hu, John Miller, and Mingze Li, "Comparative study between a new nonlinear model and common linear model for analysing laboratory simulated-forest hyperspectral data," *International Journal of Remote Sensing*, vol. 30, no. 11, pp. 2951–2962, 2009.

[13] Philip N Slater, FJ Doyle, NL Fritz, and R Welch, "Photographic systems for remote sensing," *Manual of remote sensing*, vol. 1, pp. 231–291, 1983.

[14] R Richter, D Schläpfer, and A Müller, "An automatic atmospheric correction algorithm for visible/nir imagery," *International Journal of Remote Sensing*, vol. 27, no. 10, pp. 2077–2085, 2006.